

## DESIGN OF A WEARABLE 3-DOF FOREARM EXOSKELETON FOR REHABILITATION AND ASSISTIVE PURPOSES

**Junghee Lee**

Robotics and Mechatronics Lab  
Mechanical Engineering Dept.  
Virginia Tech  
Blacksburg, VA, USA  
briellel@vt.edu

**Pinhas Ben-Tzvi**

Robotics and Mechatronics Lab  
Mechanical Engineering Dept.  
Virginia Tech  
Blacksburg, VA, USA  
bentzvi@vt.edu

### ABSTRACT

This paper presents the design and analysis of a portable forearm exoskeleton designed for rehabilitation and assistive purposes (FE.RAP). The design uses a direct-drive mechanism to actuate three degrees of freedom (DOFs) of the wrist, including: (1) wrist flexion and extension, (2) wrist radial and ulnar deviation, and (3) forearm supination and pronation. In recent decades, automated at-home recovery therapies have emerged as popular alternatives to hospital-based rehabilitation. Often in the case of lower arm rehabilitation, however, existing exoskeletons are not practical to use as home rehabilitation devices due to being non-transportable, bulky in size, and heavy in weight. In addition, compact sized exoskeletons often lack sufficient DOFs to mirror the natural movements of the hand. This paper proposes a design that addresses the drawbacks of current exoskeletons. The FE.RAP is designed to be portable and lightweight, while maintaining sufficient DOFs to help patients recover the range of motion needed by the wrist and forearm to support activities of daily living (ADL). Along with the design, the paper presents an analysis used to optimize the workspace for each DOF of the system. A kinematic analysis is performed to validate and compare the workspace of the system, as well as the coupling relationship between the DOFs, to that of the human hand and wrist. Finally, the torque required to support most ADLs is determined using static and dynamic analyses.

### 1. INTRODUCTION

A loss of hand and arm motor functions is often caused by physical injury or illness in individuals of any age. Illnesses that limit patients' activities of daily living (ADL) include metabolic bone diseases, strokes, cerebral palsy, neuromuscular disorders, and arthritis. In terms of fractures, whether caused by

physical injuries or diseases, medical studies have found that distal radius fractures, also known as wrist fracture, represents up to 1/6 of all fractures treated [1] and is one of the major osteoporotic fractures [2]. Especially for older persons, a low-impact injury such as a simple fall can easily cause a fracture due to low bone mineral density. However, metabolic bone diseases along with osteoporosis can also cause the same risk to all ages, genders, races, and ethnicities[3].

When it comes to strokes, the U.S. Department of Health and Human Services estimates that approximately 470,000 people survive strokes every year in the United States and require continuous rehabilitation to recover their motor functions [4]. Many stroke survivors who lose their motor functions also suffer emotional distress as a result of losing their independency. Relearning basic skills, such as eating and dressing, can be very stressful to some patients and failing to perform these skills without the help of others may lead to loss of confidence, thereby aggravating the condition. As a result, the use of home rehabilitation devices such as exoskeletons can help accomplish recovery while preserving the patient's independence, dignity, and self-confidence.

In addition to experiencing emotional distress, patients also suffer physical discomforts such as "frozen" joint, which causes significant pain due to the lack of movement for a prolonged period [3]. Therapists perform passive movement, gently moving or flexing a joint, to minimize the pain, but more importantly, this passive movement is known to stimulate brain sensorimotor activities [8], facilitating control of recovered motor function. Many studies continuously proved the importance of the rehabilitation robot for both rehabilitation and assistive purposes, and the positive effects of the intense rehabilitations that practice highly repetitive task-oriented

movements, are emphasized for the motor recovery and ADL [5–9].

Despite this and other research emphasize that robotic wrist rehabilitation study is imperative, insufficient consideration is given to the wrist rehabilitation compared to the amount of consideration given to the upper appendage and hand rehabilitation [10,11]. Previously, Zhou Ma worked on the five-fingered haptic glove mechanism [12]. The work presented in this paper is extension of the previous work done in Robotics and Mechatronics Lab to combine additional wrist rehabilitation support. This paper proposes a design for a forearm and wrist exoskeleton that addresses some of the drawbacks of prior exoskeletons. The FE.RAP is a portable and lightweight design that supports three DOFs of the forearm wrist: (1) wrist flexion and extension in the pitch direction, (2) wrist radial and ulnar deviation in the yaw direction, and (3) forearm supination and pronation in the roll direction. Direct-drive mechanism is used for all three DOFs as an effort to avoid issues of the cable driven mechanism [13]. As a result of having sufficient DOFs, this design is more suitable to help patients recover the essential range of motion in the forearm and wrist to support activities of daily living (ADL).

The paper is presented as follows: Section 2 provides a review of previous rehabilitation devices, Section 3 provides an overview of the mechanical design, Section 4 presents the analysis of the workspace, Section 5 presents the statics and dynamics of the system, and Section 6 concludes the paper.

## NOMENCLATURE

$R$	Max limit point of the slot towards the finger
$r$	Min limit point of the slot towards the wrist
$A$	Point of rotation of a disk
$G$	Initial point of rotation of the slider-crank
$G_n$	Unrealistic optimal point of rotation of the slider-crank
$O$	Center point of the wrist
$I$	Intersection point of two circles
$P_1$	Intersection point of the R trajectory and the slider-crank trajectory
$P_{1,n}$	The new $P_1$
$P_2$	Intersection point of the r trajectory and the slider-crank trajectory
$P_3$	Opposite corner point of $P_1$ in a diagonal of a square
$P_{PoR}$	New point of rotation of the slider-crank
$P_1P_2$	Line between the points $P_1$ and $P_2$ (mm)
$P_2P_3$	Line between the points $P_2$ and $P_3$ (mm)
$S$	Function of the line created by $P_{midpoint}$ and $CP_{square}$
$P_{midpoint}$	Midpoint of the line $P_1P_2$
$CP_{square}$	Center point of a square
$G_x$	x value of $G$ (mm)
$G_y$	y value of $G$ (mm)
$O_x$	x value of $O$ (mm)
$O_y$	y value of $O$ (mm)
$I_x$	x value of $I$ (mm)
$I_y$	y value of $I$ (mm)
$G_{n,x}$	x-coordinate of new point of rotation (mm)
$G_{n,y}$	y-coordinate of new point of rotation (mm)
$r_G$	Radius created by the slider-crank
$r_R$	Radius(distance) between R and O

$r_r$	Radius(distance) between r and O
$\theta_1$	Angle of the wrist extension ( $^\circ$ )
$\theta_2$	Angle of the wrist flexion ( $^\circ$ )
$\theta_3$	Angle between $P_2P_3$ and the horizontal line ( $^\circ$ )
$\alpha$	Passive Yaw rotation angle for the hand ( $^\circ$ )
$\beta$	Active Yaw rotation angle for the disk ( $^\circ$ )
$\gamma$	Initial angle of the $\theta_3$ ( $^\circ$ )
$\phi$	Pitch angle created by the hand at wrist ( $^\circ$ )
$\psi$	Pitch angle created by the slider-crank on the disk ( $^\circ$ )

## 2. BACKGROUND

Current robotic rehabilitation devices for the wrist can be categorized based on how patients interact with the robot: (1) stationary devices with or without a joystick on the end-effector, and (2) portable exoskeletons with or without a joystick on the end-effector. This section reviews and compares existing models for each classification described above.

### 2.1 Stationary device with or without a joystick on the end-effector

These types of rehabilitation robots do not have a size or weight limitation due to being stationary devices. The designs were mainly focused on a robustness, safety and practicality. For rehabilitation, a target position matching task was implemented via an intuitive visual interface, but the patient mainly grabbed the joystick and practiced moving a part virtually. Though virtual reality rehabilitation (VR) is rapidly becoming a popular application and has many benefits including real-time performance feedback, whether this new application is as effective as physical rehabilitation (PR) is still questionable. Patients often experience difficulties navigating in the virtual system, and [14,15] concluded that the important factor for VR to be considered as equal to PR is the sense of presence and physical environment of the performer. The examples of this class of system are Wrist Gimbal [16], WRIST device [17], RiceWrist [18], and RiceWrist-S [19]. Similarly, MARSE-4 [20], SUEFUL-6 [21], and ArmeoPower [22] are anchored to a stationary pole instead of the desk, but these devices are still not portable and used a joystick, or a palm holder for SUEFUL-6, for navigation.

Though most stationary devices used a joystick, because they normally helped survivors to practice ADL through VR, a self-aligning 3-DOF actuated exoskeleton [23] was an exceptional device. Instead of the joystick, [23] the left the hand and fingers were free to allow grabbing activities to support survivors to interact with objects physically.

### 2.2 Portable exoskeleton with or without a joystick on the end-effector

As portability became an issue and main area of improvement, several types of the portable exoskeleton were developed. Among them, a portable, yet stationary hybrid device was presented in [24]. The exoskeleton described in this paper was mounted on a mobile wheelchair for mobility. It supported 3 DOFs at the shoulder and 1 DOF of elbow motion, but the wrist was simply supported by the wrist holder and had

no actuated DOF. Though it was an innovative idea, only a portion of the patients who use wheelchair daily due to lost motor function in the legs will gain benefit from this device, and a portable exoskeleton that can be used by every patient was still needed.

Another type of devices such as SAM [25] and Exorn [26] were developed soon after [28]. SAM and Exorn were not anchored to the table or wheelchair, but despite the portability, SAM and Exorn used a joystick to control the exoskeleton. Using these devices, patients had freedom to move around the room, but were still unable to practice ADL.

The issues of immobility, bulkiness, heavy weight, and ability to use the palm were taken into consideration by many studies, and PWE[27], SCRIPT Passive orthosis[28], Looned *et al* [29] and Gilman’s robotic exoskeleton[30] were developed as a solution to these problems. These studies attempted to reduce the volume and weight while considering how the device could increase the chance of recovery by eliminating the joystick. However, often these devices had less than 3 DOFs to cover the entire Range of Motion (RoM) of a human hand. This was a major drawback of these devices because providing the essential RoM of a human hand is needed to perform ADL.

### 3. MECHANICAL DESIGN AND MODEL

When designing an exoskeleton or rehabilitation device for the wrist, its ability to support the patients to recover all 3 DOFs and the largest RoM is very important. The studies presented in [10,31] expressed how a combination of wrist and forearm postures significantly affected the wrist RoM and the finger movements. Survivors who have impaired hand motion often have difficulties controlling the wrist. Therefore, a light and portable forearm exoskeleton is desired, but most importantly, the rehabilitation device should cover the largest workspace of the human hand.

#### 3.1 Review of Human Hand Range of Motion

As mentioned in the introduction, the RoM of human hand on wrist functionality includes Pitch, Yaw, and Roll, as shown in Fig. 1. Recent studies and records [20,23,30,32–38] show a variety of RoMs. Therefore, to understand the optimal RoM of the wrist and hand, the RoM of the human hand was reviewed, and then compared to the RoMs used in other studies. The results outlined in Tables 1 and 2, show a significant variation between the data measured in 1995 and after 2000. The factors that can affect the data include gender and method used to measure the RoM [31]. The RoM measurements showed that women tend to be more flexible than men. Therefore, if the population of the data represents both men and women, having different ratios of men and women can ultimately change the final averaged measurement. The average values shown in Tables 1 and 2 were applied to the RoM used in this paper: wrist extension (60°), wrist flexion (70°), ulnar deviation (30°), radial deviation (20°), forearm pronation (90°), and forearm supination (90°). To determine the RoM to be used for the proposed design, the following facts were considered: (1)

Movable Range of the Exoskeleton should be less than the average value of the Movable Range of the Human Hand for safety, (2) Desired Movable Range of the exoskeleton could be wider than the average value of the Movable Range of the Exoskeleton, (3) average data might not be the best suitable RoM to choose due to an outlier data which could lower/raise

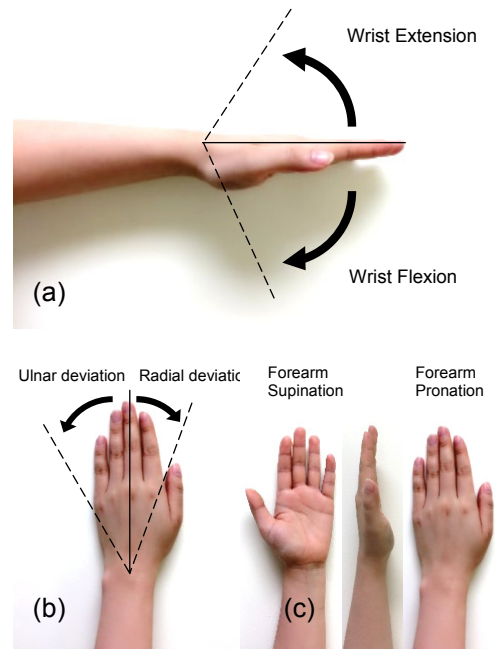


Fig. 1. Movable RoM of the hand. (a) Wrist joint: Extension and flexion, (b) Wrist joint: radial and ulnar deviation, (c) Forearm movement: Supination and Pronation

Table 1: Movable Range of Human Hand

Joint Motion [°]	Caldwell	DOD Male	DOD Female	Gopura	Gilman	Brigstocke	AVG
Wrist Extension	99	59.1	58.5	60	59.1	48	63.9
Wrist Flexion	90	78.2	83.2	70	79.8	84	80.9
Ulnar deviation	47	33.3	32.3	35	33.3	49	38.3
Radial deviation	27	26.8	26.1	25	26.4	16	24.6
Pronation		97.2	101	90			95.9
Supination		105	115	90			103.2
Pub. Year	1995	2000	2000	2008	2011	2012	

Table 2: Movable Range of Exoskeleton

JM [°]	Karim	Gopura	Gilman	Brigstocke	Beekhuis	Rahman	Stalin John	ChAR Min	AVG
WE	80	50	50	50	60	50	80	70	61.3
WF	70	60	60	45	70	60	80	70	64.4
UD	40	30	30	40	30	25	45		34.3
RD	20	20	20	15	20	20	15		18.6
Pro	135	60			80	85	90	90	90.0
Sup	90	80			90	85	80	90	85.8
PY	2004	2008	2011	2012	2013	2014	2016	2016	

the average, and (4) most used RoM could be an optimal range over the average range.

### 3.2 Initial Design

The FE.RAP was designed to have the ability to control 3 DOFs, two at the wrist and one for the forearm pronation and supination, to maximize the workspace and imitate the natural RoM of the human hand. Initially, the dimensions and positions of all the components were determined based on the average hand size of both men and women [33]. The proposed design of FE.RAP, shown in Fig. 2, is composed of a wrist bracelet, an elbow bracelet, a disk unit, and a glove unit

The wrist bracelet has 3 layers: (1) an aluminum outer layer, (2) a plastic roller bearing, and (3) a crescent cuff with silicon pads. The first layer secures the inner layers, and box clasp, also known as tab insert locking system is used for easy locking and unlocking. The second layer works as a bearing that allows the hand to be inserted through an opening, which is made up of flexible plastic. This bearing resembles a plastic conveyor with rollers, shown in Fig. 3. The slot in the middle of the bearing creates a passage for the Roll motor gear. The third layer is the innermost crescent cuff, which is designed to have gear teeth along its outer surface to create a rack and pinion mechanism with the Roll motor gear-shaft. This rack and pinion setup creates a direct drive mechanism. In addition, a silicon pad is attached to the inside of the crescent cuff to produce friction between the cuff and the arm for control while supporting a firm lock on the human arm. To maintain connection between the wrist bracelet and the disk unit during Roll motion, a sliding top is attached to the crescent cuff layer of the wrist bracelet. Ultimately, this sliding top allows for all 3 independent DOFs to be inherently coupled by allowing the Yaw and Pitch motions of the disk unit to be maintained during the Roll motions from the wrist bracelet, and vice versa.

The elbow bracelet consists of a similar outer layer, with the box clasp locking system and the silicon pad. By connecting the wrist bracelet to the elbow bracelet, the wrist bracelet is anchored to the upper part of the arm to actuate Roll motion while the second layer of the wrist bracelet rotates the wrist accordingly.

The disk unit is placed on top of the wrist bracelet and consists of a disk, a spur gear which is located under the disk

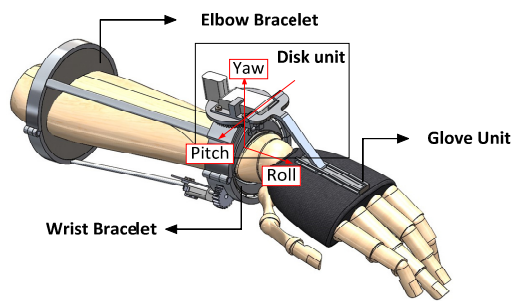


Fig. 2. Initial design of FE.RAP

that has a rack and pinion mechanism, a slider-crank bar, a slider-crank holder, and motors. As shown in Fig. 2, the spur gear is directly attached to the Yaw motor, which is placed on top of the disk vertically, producing a direct-drive for the Yaw motion. Similarly, the slider-crank is also directly attached to the Pitch motor. This direct-drive mechanism minimizes backlash from the gears, while maximizing the transmission efficiency.

The glove unit consists of a form-fitting glove for the hand to have wider RoM [39] and has a slot that is placed on the dorsal side of the glove. When the Pitch and Yaw motors are actuated, the coupled mechanism between the slider-crank bar and the slot produce Pitch and Yaw motions. A revolute joint located at the tip of the slot is added to accommodate the differences in angles between the trajectory of the disk and the hand. This modification will be explained further in Section 4.

## 4. WORKSPACE ANALYSIS

This section analyzes the workspace created by the FE.RAP. Analyses have shown that rotation about the Roll axis did not interfere with other DOFs, and the RoM for the Yaw and Roll fully covered the RoM of the human hand and the desired RoM for this research. Therefore, the focus of this analysis was devoted to the workspace of the Pitch and the Yaw motions. Following the workspace analysis, the elements including the slider-crank was modified accordingly to accommodate the change and maximize the workspace.

### 4.1 Pitch DOF

In this section, the steps taken to maximize the workspace in terms of pitch are presented. The position for the point of rotation (PoR) of the slider-crank was first selected by measuring the sample dimensions of an arm and hand. Through the workspace analysis, the RoM of the initial design was analyzed as shown in Fig. 4. The shaded area in green represents the initial RoM (45° of the wrist extension and 22° of the wrist flexion) created by the slot, and the shaded area in gray represents the initial RoM (34° of the wrist extension and 60° of the wrist flexion) created by the tip of the hand. The desired RoM of Pitch (60° wrist extension and 70° wrist flexion) is displayed in blue lines.

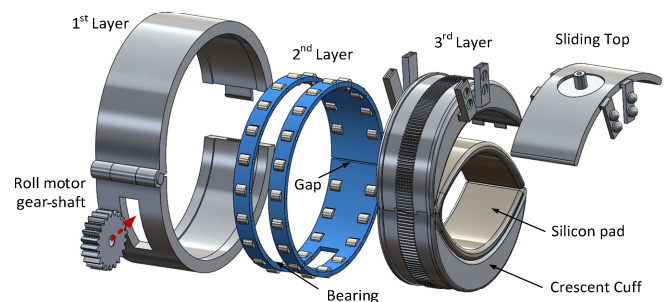


Fig. 3. Expanded view: Layers of the Wrist Bracelet

Due to the mechanical limit of the slider-crank and the slot, the Pitch RoM was limited, and the features of the initial slider-crank did not fully cover the desired RoM. To cover the maximum RoM of the hand, the position for the PoR of the slider-crank was refined through workspace optimization.

#### 4.1.1 Workspace Analysis

After trajectories created by  $R$  which is the max limit point of the slot towards the finger,  $r$ , which is the min limit point of the slot towards the wrist, and the center point of the slider-crank tip which slides on the slot (SCP) were generated, the workspace was determined by locating the intersections of the trajectories. For Pitch, the side view was considered, and Fig. 4 shows the result. Mathematically, the angle of the initial wrist extension and flexion can be expressed as

$$P_1 = (R \cos \theta_1, R \sin \theta_1) \quad (1)$$

$$P_2 = (r \cos \theta_2, -r \sin \theta_2) \quad (2)$$

$$\theta_1 = \arctan(y_1 / x_1) = \arctan(R \sin \theta_1 / R \cos \theta_1) \quad (3)$$

$$\theta_2 = \arctan(y_2 / x_2) = \arctan(-r \sin \theta_2 / r \cos \theta_2) \quad (4)$$

where  $P_1$  is the intersection point of the dashed blue arc, representing the trajectory of  $R$ , and the magenta circle, representing the trajectory of a SCP. Similarly,  $P_2$  is the intersection point of the dotted blue arc representing the trajectory of  $r$ , and the magenta circle. First, the equations representing the trajectories were written as

$$(x - G_x)^2 + (y - G_y)^2 = r_G^2 \quad (5)$$

$$(x - O_x)^2 + (y - O_y)^2 = r_R^2 \quad (6)$$

for SCP and  $R$ , and the coordinates of the intersecting points, shown in Eqs. (10) and (11), were derived via Eqs (7)-(9) using the linear equation (7). The same step can be repeated for  $r_r$  by substituting  $r_r$  into  $r_R$  in the equations.

$$y = ax + b \quad (7)$$

$$a = (-G_x - O_x) / (G_y - O_y) \quad (8)$$

$$b = (G_x^2 + G_y^2 - O_x^2 - O_y^2 - r_G^2 + r_R^2) / 2(G_y - O_y) \quad (9)$$

$$I_x = \frac{-(2ab - 2G_x - 2G_y a) + \sqrt{(2ab - 2G_x - 2G_y a)^2 - 4(1 + a^2)(b^2 - 2G_y b + G_x^2 + G_y^2 - r_G^2)}}{2(1 + a^2)} \quad (10)$$

$$I_y = b + a I_x \quad (11)$$

In Fig. 4, a black dot indicates the location of  $P_1$ , and a red dot indicates the location of  $P_2$ , along with other lines representing the RoM and the trajectories. By using the  $x$  and  $y$ -coordinates of the points, the angles of the initial RoM were calculated.

The result showed that the features of the initial design did not fully cover the desired RoM. By keeping all other features to find the optimal PoR of SCP that can cover the RoM of  $\theta_1 = 60^\circ$  and  $\theta_2 = 70^\circ$ ,  $P_1$ ,  $P_2$ , and the midpoint of  $P_1 P_2$ ,  $P_{midpoint}$ , were used to find  $\theta_3$ , which is the angle between  $P_2 P_3$  and the horizontal line. As blue lines represents the desired RoM,  $P_1$

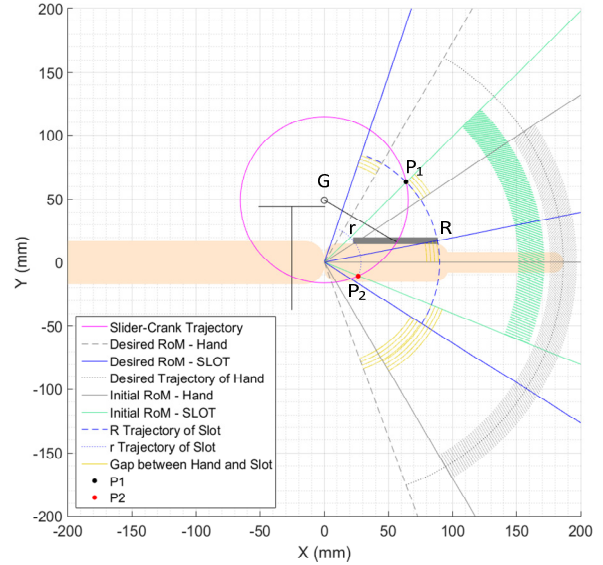


Fig. 4. Initial And Desired Workspaces of the hand and slot

and  $P_2$  in Fig. 5 are the desired intersection points. Knowing  $\theta_3$ , the coordinates of  $P_3$  and  $CP_{square}$  were calculated as

$$P_3 = (P_{1x} - P_1 P_2 \cos \theta_3, P_{1y} + P_1 P_2 \sin \theta_3) \quad (12)$$

$$CP_{square} = (P_{2x} - (P_{2x} - P_{3x}) / 2, P_{3y} - (P_{3y} - P_{2y}) / 2) \quad (13)$$

and shown in Fig. 5. As blue lines represents the desired RoM,  $P_1$  and  $P_2$  in Fig. 5 are the desired intersection points.  $S$ , the function of the line relating  $P_{midpoint}$  and  $CP_{square}$  was derived and shown in (14). By rewriting (15), the optimal value of  $G_{n,x}$  can be found with a constraint value of  $G_{n,y}$ .

$$S = (P_{my} - CP_{square,y}) / (P_{mx} - CP_{square,x}) \quad (14)$$

$$G_{n,y} = (S)G_{n,x} + [(-S)P_{mx} + P_{my}] \quad (15)$$

$$G_{n,x} = G_{n,y} - [(-S)P_{mx} + P_{my}] / S \quad (16)$$

Within the logical constraints,  $-51.32 < G_{n,x}$  (mm)  $< 0.68$  and  $G_{n,y} = 49.18$  mm, the new optimal PoR,  $G_n$ , was determined which is indicated in Fig. 5, but practically,  $G_n$  was not feasible. Therefore, the optimization of the key design parameter was required.

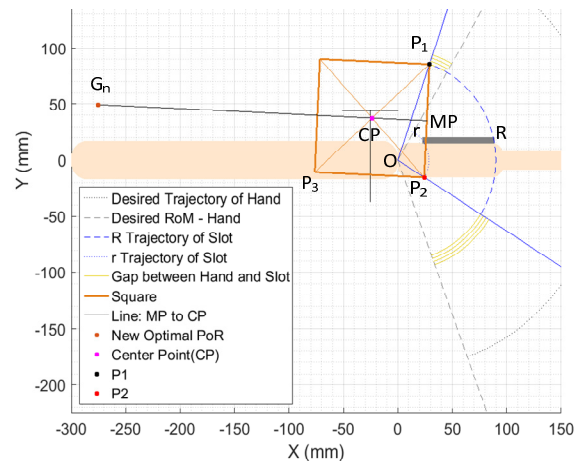


Fig. 5. Finding the optimal PoR for Pitch ( $-70^\circ/60^\circ$ )

### 4.1.2 Workspace Optimization

Thus, knowing that there is no PoR that satisfies the range of  $\theta_1 = 60^\circ$  and  $\theta_2 = 70^\circ$ , the constraint of  $\theta_1$  has changed to  $\theta_1 \leq 60^\circ$ . In consideration of flexion contracture, maximum  $\theta_2$  was preferred over maximum  $\theta_1$ . Using the equations (1)-(16) with this new constraint, the simulation was used until the first  $x$  value that satisfied all the constraint is found. As a result, the new PoR,  $P_{PoR}$ , was identified, and the  $x$  value of  $P_{PoR}$  was found to be  $-46.722$  mm from the wrist,  $O$ , as shown in Fig. 6, along with the points illustrating the optimization process. Point  $P_{I,n}$  represents the intersection point of the trajectory of the point  $R$  and the higher limit of the workspace. As the result, using the  $P_{PoR}$  location,  $\theta_1$  for the hand increased to  $49^\circ$  from  $34^\circ$ , and  $\theta_2$  increased to  $70^\circ$  from  $60^\circ$ . The wrist extension angle at  $P_{I,n}$  for the slot is about  $60.23^\circ$  due to the offset angle which is about  $11.23^\circ$ . This offset angle is an angle between the palm and the plane created by  $R$  and  $O$ . Due to the differences in radii and PoR of three trajectories of the SCP,  $R$  and  $r$ , the offset continuously changes from  $P_1$  to  $P_2$ . As the SCP slides on the slot and changes its position along the Pitch motion, when the SpC reaches  $P_2$  (the maximum wrist flexion position), the offset would be measured from the plane created by  $r$  and  $O$ . This change increases the offset up to  $37.69^\circ$ . In addition, the

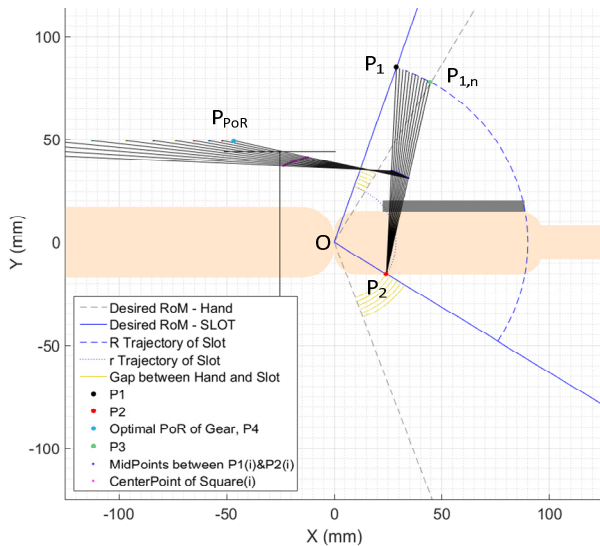


Fig. 6. Optimization of PoR

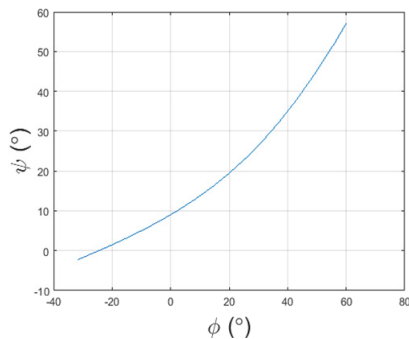


Fig. 7. The relationship between the angle  $\phi$  and  $\psi$  created by the Pitch

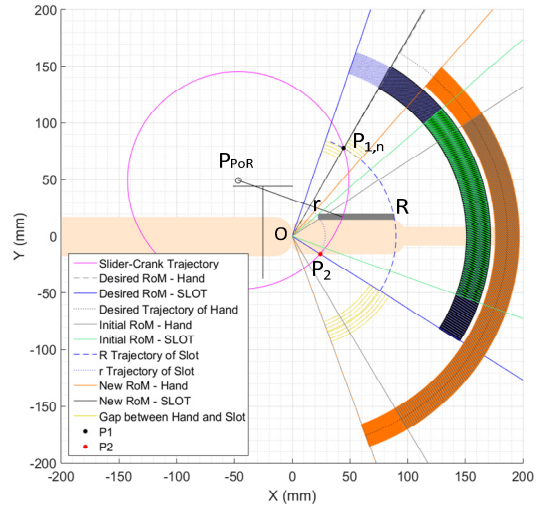


Fig. 8. Comparison between the initial and the new workspace

relationship between the Pitch angle created by the hand at the wrist,  $\phi$ , and the Pitch angle created by the slider-crank bar on the disk,  $\psi$ , is illustrated in Fig. 7.

Finally, Fig.8 compares the ranges of the workspace from the side view. The PoR position is updated to the  $P_{PoR}$  position, and the new  $P_{I,n}$  and  $P_2$  points are marked. The shaded black region under the green and blue regions represents the optimized workspace for the slot, while the shaded orange region represents the workspace for the hand.

By changing other key components, achieving a wrist extension of  $60^\circ$  was also possible, but those considerable options were questioned for practicality reasons. Details of the options and the reason to overrule these options are explained in Section 5.3.

### 4.2 Yaw DOF

Assuming that the tip of the middle finger (ToF) aligns in the mid plane of the palm, the line from the center of the wrist (CoW) to the ToF and the vertical mid plane of the slot should be collinear. A challenge arose when the Yaw workspace was analyzed. The coupled mechanism between the PoR of the disk and the PoR of the wrist affected the Yaw RoM. To address this challenge, the trajectories created by ToF with respect to the wrist and SCP with respect to the disk were analyzed to find the interference between the wrist and the disk.

#### 4.2.1 Workspace Analysis

The top view shown in Fig. 9 illustrates the maximum radial deviation ( $20^\circ$ ) of the hand and the slider-crank on the disk. The wrist rotates about  $O$ , and the disk rotates about  $A$ . With the hand length,  $L_{HAND}$ , the red dashed circle represents the trajectory of ToF. Similarly, the green line represents the trajectory created by the SCP with  $L_{CRANK}$ . The  $OC$  represents the line created between the CoW and the ToF at initial configuration ( $0^\circ$ ), and the  $OD$  represents  $OC$  at the maximum radial deviation ( $20^\circ$ ). The PoR will follow the trajectory of the Disk as it is located on top of the Disk, but two different

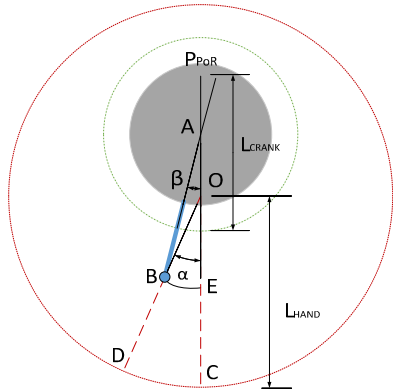


Fig. 9. Top View: Trajectories Of the radial deviation (20°)

points of rotation,  $A$  and  $O$ , create the angle difference between  $\alpha$ , the passive Yaw rotation angle for the hand, and  $\beta$ , the active Yaw rotation angle for the Disk. The arc length equation of  $BE$  is rearranged to find the ratio of  $\alpha$  and  $\beta$  as

$$\alpha(L_{HAND}) = \beta(L_{CRANK}) \quad (17)$$

### 4.3 Optimized Design

The key design parameters were modified to reflect the results found from the workspace analysis, and Fig. 10 shows the modified design. The PoR was relocated to the  $P_{PoR}$ , and to accommodate this change, the slider-crank design was

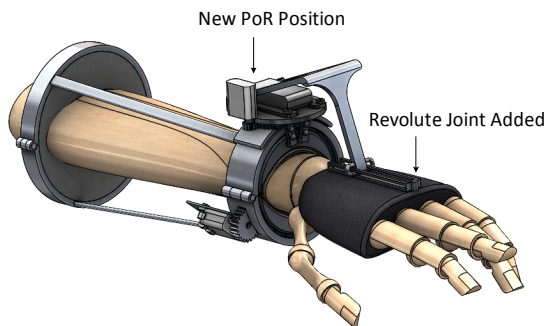


Fig. 10. Modified Design of FE.RAP

modified. The motor for the Yaw was replaced to the side to accommodate the relocation of PoR. Also, a revolute joint was added to the tip of the slot as the slot always has to be parallel to the slider-crank. This addition would allow the coupled mechanism between two angles.

Previously, considerable options to facilitate full RoM were briefly mentioned. Key options to achieve a wrist extension of 60° include (1) extending the tip of the slot and (2) changing the  $G_{n,y}$  constraint. The first approach would result in protrusion of the slot from the hand. Though a wrist extension of 60° was guaranteed, the idea was overruled due to the safety reason and possible discomfort. The second option can be investigated in the future after the motor selection. Once the motor is sized, according to the shaft height from the disk, new  $G_{n,y}$  constraint can be considered. Lowering the  $G_{n,y}$  also is a

solution to guarantee wrist extension of 60°, but the position of the motor would be a challenge.

## 5. STATICS AND DYNAMICS

The kinematic model representing FE.RAP was created to establish Denavit-Hartenberg (DH) Parameters, and the link frames of the system are depicted in Fig. 11. The rotation around  $Z_1$  actuates Roll,  $Z_2$  actuates Yaw, and  $Z_3$  actuates Pitch. For this paper, SCP was considered to be the end-effector point for simplicity.

### 5.1 Kinematic Analysis

In this section, two types of analyses are presented. The first analysis used forward kinematics to illustrate the 3D workspace by the end-effector point, SCP. Depending on the fingers configuration of a patient, the workspace of ToF can change, but the workspace of SCP presented in this section will not change. By computing 3D workspace, the coupling relationship between the DOFs is also reviewed in this section. The second analysis studies the relationship between the force applied to the end-effector and the torque produced at the joints to hold the hand in a static equilibrium.

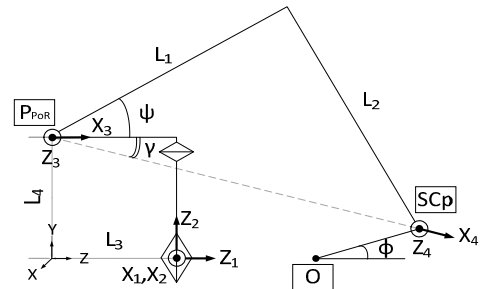


Fig. 11. The side view of the kinematic model of FE.RAP

#### 5.1.1 Forward Kinematics

To formulate the forward kinematics problem, the DH parameters shown in Table 3 and transformation matrices were established from the kinematic model. The SCP positions with respect to the wrist coordinate frame were computed and displayed in Fig. 12. These positions represent the workspace created by Pitch and Yaw motions in 3D. Pitch created the vertical curves, and yaw created horizontal curves. Combining these two motions created a curved surface and the construction of color from light pink to dark blue shows the 1° increment of yaw motion from 30° ulnar deviation to 20° radial deviation. In addition, 1° increment for Pitch was used. The crank-slider figure is at 49° wrist extension on top and 70° wrist flexion on the bottom.

Using the RoM for 3 DOFs verified from Section 4,

Table 3: DH Parameters

$i$	$a$	$\alpha$	$d_i$	$\theta_i$
1	0	90°	0	$\theta_{Roll}$
2	$L_2$	90°	$L_1$	$\theta_{Yaw} + 90^\circ$
3	$L_3$	0°	0	$\theta_{Pitch} - \gamma$

additional workspace which has all 3 DOF's including Roll was illustrated. As a result, the surface shown in Fig. 12 was rotated about the Roll axis and created a full workspace of FE.RAP in 3D as shown in Fig.13. The construction of the colors from light pink to dark blue represents 2° rotation increment of the Roll DOF from forearm pronation to supination. Though Roll is for 180° in total, the workspace seems to rotate more than that due to the Yaw motion.

Recent studies on human factors revealed that combination of wrist and forearm postures have effects on wrist RoM [31]. The combinations of Pitch and Yaw affected, and reduced the workspace. From Fig. 13 and Fig. 14, this coupled mechanism was confirmed. As the angles of wrist extension and flexion increased from 0°, the ulnar and wrist deviation displacement decreased in value as expected.

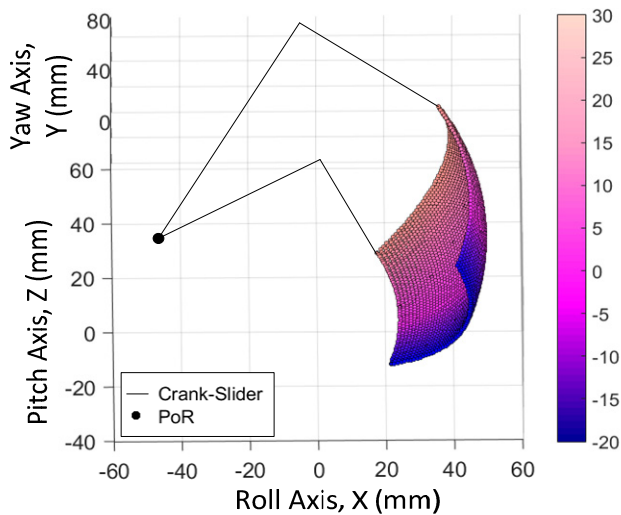


Fig. 12. Pitch and Yaw Workspace without Roll motion

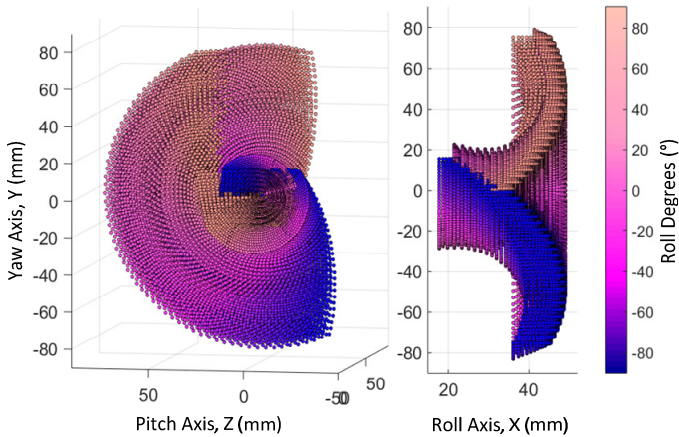


Fig. 13. 3DOF: Pitch, Yaw, Roll Workspace

### 5.1.2 Statics Modeling and Analysis

To understand what torque is necessary to hold a hand in static equilibrium, the manipulator statics relationship was evaluated. Assuming the frictional forces at the joints are

negligible, if there is a static equilibrium, the total work produced by the force and joint torque of the hand is zero. After locating the center of mass of three parts (CoM): (1) the slider-crank bar, (2) the slot, and (3) the hand, the force and moment vectors applied at CoM were computed. Based on the force and moment vectors applied at the CoM, the equivalent force and moment at the SCP was derived. Knowing the SCP positions with respect to the wrist coordinate frame, the Jacobian at the static equilibrium was derived. Hence, the torque applied to the SCP can be expressed as

$$\tau = -{}^0J_{SCP}^T {}^0F \quad (18)$$

where  $\tau$  is a joint torque vector,  ${}^0J$  is a 6×3 Jacobian matrix relating joint displacements to the hand displacements, and  ${}^0F$  is an external generalized force applied to the SCP.

Approximately, the slider-crank bar's mass is calculated to be 0.02786 kg if 6061 aluminum alloy is used. Similarly, the 6061 aluminum alloy slot will approximately have a mass of 0.00369 kg. For the hand, knowing that the hand is 0.66% of the body mass [40], the maximum of averages of different races [41] was used to get the mass of the hand, which is 0.61314 kg. As a result, the required torque to hold a hand in static equilibrium is

$$\tau = \begin{bmatrix} \tau_{Roll} \\ \tau_{Yaw} \\ \tau_{Pitch} \end{bmatrix} = \begin{bmatrix} .0439 \\ 0 \\ .5724 \end{bmatrix} Nm \quad (19)$$

### 5.1.3 Dynamics Modeling and Analysis

Considering the external generalized force expressed in the wrist frame, the dynamic equation of motion for FE.RAP is derived using Lagrangian method, and can be expressed as

$$M(q)\ddot{q} + C(q, \dot{q})\dot{q} + G(q) - {}^0J_{SCP}^T {}^0F_{ext} = \tau \quad (20)$$

where  $q, \dot{q}, \ddot{q}$  are the joint displacement, velocity, and acceleration, respectively,  $M(q)$  is a 3×3 inertia matrix,  $C(q, \dot{q})$  is a 3×3 Coriolis matrix,  $G(q)$  is a 3×1 matrix of gravity effects,  ${}^0J$  is a 6×3 Jacobian matrix expressed in the base frame,  ${}^0F_{ext}$  is a 6×1 matrix of external generalized force applied at the hand expressed in the base frame, and  $\tau$  is a 3×1 matrix of joint torques.

Without an additional mass on the hand, the torque at the joints needed to move the hand can be expressed as

$$\tau = \begin{bmatrix} \tau_{Roll} \\ \tau_{Yaw} \\ \tau_{Pitch} \end{bmatrix} = M \begin{bmatrix} \ddot{\theta}_1 \\ \ddot{\theta}_2 \\ \ddot{\theta}_3 \end{bmatrix} + C \begin{bmatrix} \dot{\theta}_1 \\ \dot{\theta}_2 \\ \dot{\theta}_3 \end{bmatrix} + G \quad (21)$$

and  $\tau_{Pitch}$  can be illustrated in Fig. 14. In reality, the angle of the elbow would also need to be considered, but to compute the torque for this section, the forearm is assumed to be parallel to the ground. The range of Pitch angles shown in Fig. 14 represents  $\psi$ . When  $\Theta_1$  is 0°, the hand would be parallel to the ground. At the angle 0°, the torque is at a maximum due to the

90° angle created between the force and the hand. When extra mass such as 1L bottle of water is held by the hand, the maximum torque would increase to about 1.8 Nm.

Since the force due to gravity is considered, in theory, there is no direct force applied to the Yaw or Roll. Only considering the moment of inertia applied to the axis of rotation, the torque for the Yaw and Roll were computed, but they were insignificantly small.

## 6. CONCLUSION AND FUTURE WORK

This paper presented the design and analysis of FE.RAP, a 3-DOFs portable and wearable forearm exoskeleton for rehabilitation and assistive purposes. The FE.RAP combines crucial design requirements such as compactness, reduced weight, wear-ability and the existence of all required 3 DOFs. Profound consideration was given to the interface between the exoskeleton and the human. As a result, use of a joystick was avoided. Instead, the top of the hand was used with a slider-crank mechanism to actuate Pitch. The design was validated through the analyses of the workspace and forward kinematics.

Future work associated with this topic includes studies into improving the range of motion, improving the mechanics model, applying the model for control, and prototype development. In terms of improving the range of motion, more practicable options to further increase the wrist extension to 60° are needed to be considered and verified. In terms of improving the mechanics model, the key step is reducing the volume of the system. In addition, if mechanics model modification would be required to cover the wrist extension of 60°, the necessary change can be implemented to the model by optimizing the structural components design. To apply the model for control, the next key step is developing the controller. Sensing and localization strategies need to be developed. The prototypes resulting from the designs discussed in this paper will be used in part to experimentally validate the concept and future associated work. Future investigations into control will explore ways to interact with patients, but before applying the prototype on a human subject, FE.RAP would be validated through experiments. Once FE.RAP is validated to be safe, further experiments can be conducted with patients.

## REFERENCES

- [1] Black, W. S., and Becker, J. a, 2009, "Common Forearm Fractures in Adults.," *Am. Fam. Physician*, **80**(10), pp. 1096–102.
- [2] Unnanuntana, A., Gladnick, B. P., Donnelly, E., and Lane, J. M., 2010, "The Assessment of Fracture Risk," *J. Bone Jt. Surgery-American Vol.*, **92**(3), pp. 743–753.
- [3] Dipiro, J. et al, 2008, "Summary for Policymakers," *Climate Change 2013 - The Physical Science Basis*, Intergovernmental Panel on Climate Change, ed., Cambridge University Press, Cambridge, pp. 1–30.
- [4] 2014, *Post-Stroke Rehabilitation*, National Institutes of Health.
- [5] Bütetfisch, C., Hummelsheim, H., Denzler, P., and Mauritz, K.-H., 1995, "Repetitive Training of Isolated Movements Improves the Outcome of Motor Rehabilitation of the Centrally Paretic Hand," *J. Neurol. Sci.*, **130**(1), pp. 59–68.
- [6] Aisen, M. L., Krebs, H. I., Hogan, N., McDowell, F., and Volpe, B. T., 1997, "The Effect of Robot-Assisted Therapy and Rehabilitative Training on Motor Recovery Following Stroke," *Arch. Neurol.*, **54**(4), pp. 443–446.
- [7] Lam, P., Hebert, D., Boger, J., Lacheray, H., Gardner, D., Apkarian, J., and Mihailidis, A., 2008, "A Haptic-Robotic Platform for Upper-Limb Reaching Stroke Therapy: Preliminary Design and Evaluation Results," *J. Neuroeng. Rehabil.*, **5**(1), p. 15.
- [8] Kwakkel, G., Wagenaar, R. C., Koelman, T. W., Lankhorst, G. J., and Koetsier, J. C., 1997, "Effects of Intensity of Rehabilitation After Stroke : A Research Synthesis," *Stroke*, **28**(8), pp. 1550–1556.
- [9] Cifu, D. X., and Stewart, D. G., 1999, "Factors Affecting Functional Outcome after Stroke: A Critical Review of Rehabilitation Interventions," *Arch. Phys. Med. Rehabil.*, **80**(5), pp. S35–S39.
- [10] Squeri, V., Masia, L., Giannoni, P., Sandini, G., and Morasso, P., 2014, "Wrist Rehabilitation in Chronic Stroke Patients by Means of Adaptive, Progressive Robot-Aided Therapy," *IEEE Trans. Neural Syst. Rehabil. Eng.*, **22**(2), pp. 312–325.
- [11] Ma, Z., Ben-Tzvi, P., and Danoff, J., 2016, "Hand Rehabilitation Learning System With an Exoskeleton Robotic Glove," *IEEE Trans. Neural Syst. Rehabil. Eng.*, **24**(12), pp. 1323–1332.
- [12] Ma, Z., Ben-Tzvi, P., and Danoff, J., 2014, "Modeling Human Hand and Sensing Hand Motions With the Five-Fingered Haptic Glove Mechanism," *Volume 5A: 38th Mechanisms and Robotics Conference*, ASME, p. V05AT08A008.
- [13] Rahman, M. H., Rahman, M. J., Cristobal, O. L., Saad, M., Kenné, J. P., and Archambault, P. S., 2015, "Development of a Whole Arm Wearable Robotic Exoskeleton for Rehabilitation and to Assist Upper Limb Movements," *Robotica*, **33**(1), pp. 19–39.
- [14] Keshner, E. A., 2004, "Virtual Reality and Physical Rehabilitation: A New Toy or a New Research and Rehabilitation Tool?," *J. Neuroeng. Rehabil.*, **1**(1), p. 8.
- [15] Stanney, K., and Salvendy, G., 1998, "Aftereffects and Sense of Presence in Virtual Environments: Formulation of a Research and Development Agenda," *Int. J. Hum. Comput. Interact.*, **10**(2), pp. 135–187.
- [16] Martinez, J. A., Ng, P., Son Lu, Campagna, M. S., and Celik, O., 2013, "Design of Wrist Gimbal: A Forearm and Wrist Exoskeleton for Stroke Rehabilitation," *2013 IEEE 13th International Conference on Rehabilitation Robotics (ICORR)*, IEEE, pp. 1–6.
- [17] Cappello, L., Contu, S., Elangovan, N., Khosravani, S., Konczak, J., and Masia, L., 2014, "Evaluation of Wrist Joint Proprioception by Means of a Robotic Device," *2014 11th International Conference on Ubiquitous Robots and Ambient Intelligence (URAI)*, IEEE, pp. 531–534.
- [18] Gupta, A., O'Malley, M. K., Patoglu, V., and Burgar, C., 2008, "Design, Control and Performance of RiceWrist: A Force Feedback Wrist Exoskeleton for Rehabilitation and Training," *Int. J. Rob. Res.*, **27**(2), pp. 233–251.
- [19] Pehlivan, A. U., Lee, S., and O'Malley, M. K., 2012, "Mechanical Design of RiceWrist-S: A Forearm-Wrist

- Exoskeleton for Stroke and Spinal Cord Injury Rehabilitation,” *2012 4th IEEE RAS & EMBS International Conference on Biomedical Robotics and Biomechanics (BioRob)*, IEEE, pp. 1573–1578.
- [20] Rahman, M. H., K-Ouimet, T., Saad, M., Kenne, J. P., and Archambault, P. S., 2011, “Control of a Powered Exoskeleton for Elbow, Forearm and Wrist Joint Movements,” *2011 IEEE International Conference on Robotics and Biomimetics*, IEEE, pp. 1561–1566.
- [21] Gopura, R. A. R. C., Kiguchi, K., and Li, Y., 2009, “SUEFUL-7: A 7DOF Upper-Limb Exoskeleton Robot with Muscle-Model-Oriented EMG-Based Control,” *2009 IEEE/RSJ International Conference on Intelligent Robots and Systems*, IEEE, pp. 1126–1131.
- [22] Lu, E. E. C., 2011, “Development of an Upper Limb Robotic Device for Stroke Rehabilitation.”
- [23] Beekhuis, J. H., Westerveld, A. J., van der Kooij, H., and Stienen, A. H. A., 2013, “Design of a Self-Aligning 3-DOF Actuated Exoskeleton for Diagnosis and Training of Wrist and Forearm after Stroke,” *2013 IEEE 13th International Conference on Rehabilitation Robotics (ICORR)*, IEEE, pp. 1–5.
- [24] Kiguchi, K., Rahman, M. H., Sasaki, M., and Teramoto, K., 2008, “Development of a 3DOF Mobile Exoskeleton Robot for Human Upper-Limb Motion Assist,” *Rob. Auton. Syst.*, **56**(8), pp. 678–691.
- [25] Letier, P., Avraam, M., Veillerette, S., Horodinca, M., De Bartolomei, M., Schiele, A., and Preumont, A., 2008, “SAM : A 7-DOF Portable Arm Exoskeleton with Local Joint Control,” *2008 IEEE/RSJ International Conference on [26] Manna, S. K., and Bhaumik, S., 2013, “A Bioinspired 10 DOF Wearable Powered Arm Exoskeleton for Rehabilitation,” J. Robot.*, **2013**, pp. 1–15.
- [27] Xiao, Z. G., and Menon, C., 2011, “Towards the Development of a Portable Wrist Exoskeleton,” *2011 IEEE International Conference on Robotics and Biomimetics*, IEEE, pp. 1884–1889.
- [28] Ates, S., Haarman, C. J. W., and Stienen, A. H. A., 2017, “SCRIPT Passive Orthosis: Design of Interactive Hand and Wrist Exoskeleton for Rehabilitation at Home after Stroke,” *Auton. Robots*, **41**(3), pp. 711–723.
- [29] Looned, R., Webb, J., Xiao, Z., and Menon, C., 2014, “Assisting Drinking with an Affordable BCI-Controlled Wearable Robot and Electrical Stimulation: A Preliminary Investigation,” *J. Neuroeng. Rehabil.*, **11**(1), p. 51.
- [30] Gilman, C. V., Ben-Tzvi, P., Yessin, G., and Danoff, J., 2011, “A Robotic Exoskeleton Device for Augmenting Wrist Movement and Grip Function in Debilitated Patients,” *ASME 2011 International Mechanical Engineering Congress and Exposition*, ASME, pp. 1041–1050.
- [31] Marshall, M. M., Mozrall, J. R., and Shealy, J. E., 1999, “The Effects of Complex Wrist and Forearm Posture on Wrist Range of Motion,” *Hum. Factors J. Hum. Factors Ergon. Soc.*, **41**(2), pp. 205–213.
- [32] Caldwell, D. G., Kocak, O., and Andersen, U., 1995, “Multi-Armed Dexterous Manipulator Operation Using Glove/exoskeleton Control and Sensory Feedback,” *Proceedings 1995 IEEE/RSJ International Conference on Intelligent Robots and Systems. Human Robot Interaction and Cooperative Robots*, IEEE Comput. Soc. Press, pp. 567–572.
- [33] 2000, *Human Engineering Design Data Digest*, DEPARTMENT OF DEFENSE HUMAN FACTORS ENGINEERING TECHNICAL ADVISORY GROUP.
- [34] Brigstocke, G., Hearnden, A., Holt, C. A., and Whatling, G., 2013, “The Functional Range of Movement of the Human Wrist,” *J. Hand Surg. (European Vol.)*, **38**(5), pp. 554–556.
- [35] Abdel-Malek, K., Yang, J., Brand, R., and Tanbour, E., 2004, “Towards Understanding the Workspace of Human Limbs,” *Ergonomics*, **47**(13), pp. 1386–1405.
- [36] Gopura, R. A. R. C., and Kiguchi, K., 2008, “Development of a 6DOF Exoskeleton Robot for Human Upper-Limb Motion Assist,” *2008 4th International Conference on Information and Automation for Sustainability*, IEEE, pp. 13–18.
- [37] John, M. R. S., Thomas, N., and Sivakumar, V. P. R., 2016, “Design and Development of Cable Driven Upper Limb Exoskeleton for Arm Rehabilitation,” *Int. J. Sci. Eng. Res.*, **7**(3), pp. 1432–1440.
- [38] Keller, U., van Hedel, H. J. A., Klamroth-Marganska, V., and Riener, R., 2016, “ChARMin: The First Actuated Exoskeleton Robot for Pediatric Arm Rehabilitation,” *IEEE/ASME Trans. Mechatronics*, **21**(5), pp. 2201–2213.
- [39] Ben-Tzvi, P., Danoff, J., and Ma, Z., 2016, “The Design Evolution of a Sensing and Force-Feedback Exoskeleton Robotic Glove for Hand Rehabilitation Application,” *J. Mech. Robot.*, **8**(5), p. 51019.
- [40] Tözeren, A., 2000, *Human Body Dynamics: Classical Mechanics and Human Movement*, Springer.
- [41] Fryar, C. D., Gu, Q., and Ogden, C. L., 2016, “Anthropometric Reference Data for Children and Adults: United States, 2011-2014,” *Natl. Cent. Heal. Stat. Vital Heal. Stat.* (3(39)), pp. 1–46.